

Direct Photo-Patterning of Efficient and Stable Quantum Dot Light-Emitting Diodes via Light-Triggered, Carbocation-Enabled Ligand Stripping

Zhong Fu, Likuan Zhou, Yue Yin, Kangkang Weng, Fu Li, Shaoyong Lu, Dan Liu, Wenyong Liu, Longjia Wu, Yixing Yang, Haifang Li, Lian Duan, Hai Xiao, Hao Zhang*, and Jinghong Li*



Cite This: *Nano Lett.* 2023, 23, 2000–2008



Read Online

ACCESS |

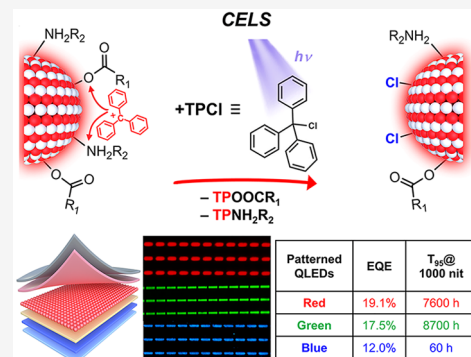
Metrics & More

Article Recommendations

Supporting Information

ABSTRACT: Next generation displays based on quantum dot light-emitting diodes (QLEDs) require robust patterning methods for quantum dot layers. However, existing patterning methods mostly yield QLEDs with performance far inferior to the state-of-the-art individual devices. Here, we report a light-triggered, carbocation-enabled ligand stripping (CELS) approach to pattern QLEDs with high efficiency and stability. During CELS, photogenerated carbocations from triphenylmethyl chlorides remove native ligands of quantum dots, thereby producing patterns at microscale precision. Chloride anions passivate surface defects and endow patterned quantum dots with preserved photoluminescent quantum yields. It works for both cadmium-based and heavy-metal-free quantum dots. CELS-patterned QLEDs show remarkable external quantum efficiencies (19.1%, 17.5%, 12.0% for red, green, blue, respectively) and a long operation lifetime (T_{95} at 1000 nits up to 8700 h). Both are among the highest for patterned QLEDs and approach the records for nonpatterned devices, which makes CELS promising for building high-performance QLED displays and related integrated devices.

KEYWORDS: quantum dots, photopatterning, light-emitting diodes, photochemistry, ligand chemistry



Colloidal quantum dots (QDs) have emerged as prominent building blocks for next generation electronic, optoelectronic, and photonic devices.^{1–3} In particular, QD-based light-emitting diodes (QLEDs) show a compelling combination of bright electroluminescence (EL), exceptional color purity, and ultrathin form factors, thereby rendering them competitive for next generation displays.^{4–8} Recent efforts on QD chemistry and device engineering have led to individual devices with EL characteristics suitable for widespread applications.¹ For reference, the record external quantum efficiencies (EQEs) of individual red,⁹ green,¹⁰ and blue¹¹ QLEDs all exceed 20%, which approaches their theoretical limits. State-of-the-art individual QLEDs also show a long operation lifetime. T_{95} , or the time for the initial brightness to decay to 95%, at 1000 nit (i.e., 1000 cd m⁻²) is ~4000, ~2500, and ~40 h for red,¹² green,¹⁰ and blue¹¹ devices, respectively.

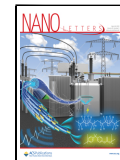
In contrast to the remarkable advances at the material and individual device level, the development of QD patterning methods that do not cause cross-contamination or device degradation remains challenging.^{5,13,14} Such patterning methods are prerequisites for incorporating QLEDs in system-level platforms, especially high-definition displays and wearable virtual/augmented reality devices. The patterning of QD layers is typically realized by using two categories of technologies. (i)

Conventional patterning methods largely inherit techniques developed for traditional inorganic semiconductor layers (e.g., photolithography^{15,16} and transfer printing^{17,18}) and solution-processed organic materials (e.g., inkjet printing),¹⁹ with their modifications entailing electrically²⁰ or chemically²¹ prepatterned substrates/stamps.^{22,23} They suffer from trade-offs in the patterning efficiency, resolution, and degraded properties of patterned QDs due to chemical/mechanical incompatibilities. Patterned QLEDs show EQEs (up to ~14.7% for red QLEDs²³) that are much lower than the best individual (or nonpatterned) devices. (ii) Direct photopatterning methods via designed surface photochemistry^{13,24–30} are built on two core concepts of QDs: namely, the surface chemistry and colloidal stability, and enable photolithographic patterning of QDs in the absence of traditional photoresists. Despite the impressive versatility, the ligand photochemistry involved in direct photopatterning, mostly on the basis of photo-

Received: January 11, 2023

Revised: February 18, 2023

Published: February 24, 2023



decomposable ligands or photo-cross-linkers, profoundly affects the photophysical properties of patterned QDs via various factors, including radicals and surface traps.³⁰ This leads to moderate EL characteristics of patterned QLEDs (e.g., EQEs for blue, ~3%; green, ~6%; red, 14.6%).^{25,26,30} A recent work developed photopatternable QDs with dual ligands, where the introduced benzophenone-containing ligands enabled patterned QLEDs with high EQEs (red, ~20%; green, ~15%).²⁷ The design of material-tailored ligand photochemistry is, thus, critical for patterning QLEDs without degraded performance.

In this work, we introduce a direct photopatterning method for building patterned QLEDs that match directly the state-of-the-art, nonpatterned devices in both efficiency and device stability. This method relies on a new ligand photochemistry, namely, the light-triggered, carbocation-enabled ligand stripping (or CELS) of QDs. CELS uses a small amount (~2 wt %) of light-sensitive triphenylmethyl chloride (TPCl) or similar chemicals as additives to QD films. TPCL photodissociates to form triphenylcarbonium cations (TP^+) and chloride anions (Cl^-) that play dual roles in CELS. On the one hand, the local release of Lewis acidic TP^+ cations readily removes native ligands from the QD surface in close proximity and reduces their solubility in nonpolar solvents, thereby producing patterns with high lateral resolution (~4 μm). On the other hand, the Lewis basic Cl^- anions effectively bind to metal sites on the QD surface and passivate defects, as supported by both experimental and modeling results. This surface chlorination endows patterned QD layers with unaltered photoluminescent quantum yields (PLQYs) and even improves photostability compared with pristine QDs. CELS is versatile to various QDs, including the cadmium-based and heavy-metal-free QDs with different native ligands. The nondestructive nature allows CELS to build efficient and stable patterned QLEDs. High EQEs and a long lifetime (T_{95} at 1000 nit) are achieved for red (19.1%, 7600 h), green (17.5%, 8700 h), and blue (12.0%, 60 h) patterned QLEDs. These values outperform those reported for patterned QLEDs (Table S1) and approach the records for the state-of-the-art, nonpatterned devices. CELS and the associated photochemistry represent as a promising, material-tailored patterning method toward advanced pixelated QLED displays and related integrated QD devices.

Photochemistry of CELS. The core of CELS is the light-triggered ligand stripping of QDs with TPCL as photosensitive additives (Figure 1). TPCL has a large molar extinction coefficient in the deep UV region (~ $1.0 \times 10^3 \text{ cm}^{-1} \text{ M}^{-1}$ at 254 nm, Figure S1) and high solubility in nonpolar solvents. This facilitates the preparation of films from a mixed solution of TPCL and QDs. During CELS, TPCL photodissociates to form TP^+ cations and Cl^- anions under UV irradiation (Figure 1A). TP^+ are strong Lewis acids³¹ that can effectively remove the nucleophilic native organic ligands (typically oleic acid, OA; oleylamine, OLA; and alkyl thiols) from the QD surface.^{31,32} QDs with reduced ligand density lose their colloidal stability (Figure S2), as qualitatively rationalized by the classic³³ or the intermolecular entropy model.³⁴ This photochemical ligand stripping process and the strongly altered colloidal stability set the basis of QD patterning. Concurrently, the Lewis basic Cl^- ions bind to the electrophilic metal sites on QD surface and passivate defects generated because of ligand removal. This surface chlorination process preserves the photophysical properties of QDs (with a mixture of native and Cl^- ligands) and improves their photostability, which

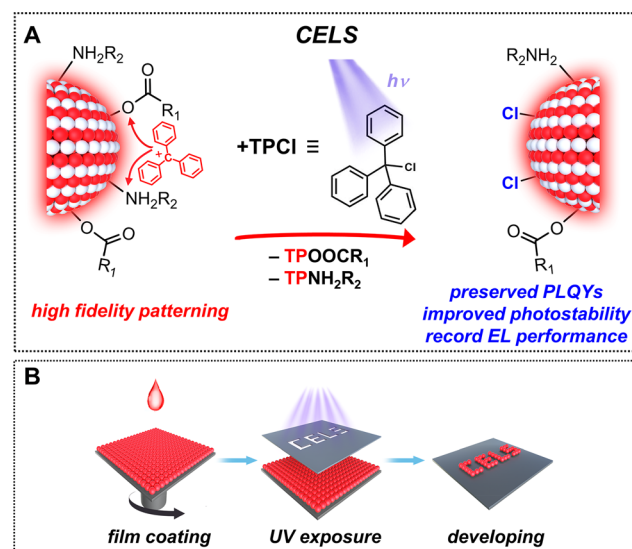


Figure 1. Schematic illustration of CELS. (A) Photochemistry involved in CELS. TPCL photodissociates under 254 nm and produces TP^+ and Cl^- . The Lewis acidic TP^+ cations readily remove the native ligands (alkyl carboxylates or amines, abbreviated as R_1COO^- and R_2NH_2^- , and also other conventional QD ligands, such as alkyl thiols) from the QD surface by forming corresponding adducts (TPOOCCR_1 and TPNH_2R_2). This leads to a loss of colloidal stability and permits high-fidelity patterning. Cl^- anions then bind to the undercoordinated metal sites to passivate surface defects, thereby leading to QDs with mixed ligands, unaltered PLQYs and enhanced photostability, and record EL performance. (B) Procedures for CELS.

ultimately leads to efficient and stable patterned QLEDs. The procedures for CELS contain three steps (Figure 1B): (i) film coating from an ink of QDs and TPCL, (ii) UV exposure via predesigned photomasks to trigger the local TPCL photochemistry in exposed regions, and (iii) removal of unexposed QDs with developer solvents (typical nonpolar solvents, such as toluene) and the formation of QD patterns.

The chemistry described above, including (i) the photo-generation of TP^+ , (ii) their electrophilic reaction with native ligands on QDs (i.e., ligand stripping), and (iii) surface chlorination, can be validated by spectroscopic analysis (Figure 2). II–VI core/shell QDs (Figure S3) and Au nanocrystals with their native ligands were used as model systems. Because all these processes occur at the QD surface, the results shown on these models can be extended to other nanocrystals. UV-visible absorption spectrum of UV-exposed TPCL solution in dichloromethane (Figure 2A) shows two peaks at 415 and 439 nm, which is characteristic for TP^+ in the presence of TP^+ -stabilizers.^{35,37} Prior to UV exposure, TPCL shows weak absorption features, presumably because of its equilibrium between the molecular and dissociated forms. The contrast in absorption spectra before and after UV exposure confirms the photogeneration of TP^+ .

TP^+ can readily react with strong Lewis bases, such as OLA, as confirmed by the disappearance of their absorption features (black curve in Figure 2A). More evidence for this reaction was provided by matrix-assisted laser desorption/ionization time-of-flight mass spectrometry (MALDI–TOF MS) results. The mixture of TPCL and OLA produces an adduct (TP–OLA) after UV exposure (Figure 2B and Figure S4). The mass peak ($m/z = 510.77$) and peak intensity distribution of this adduct correlate well with the simulated results for $(\text{C}_6\text{H}_5)_3\text{C}-$

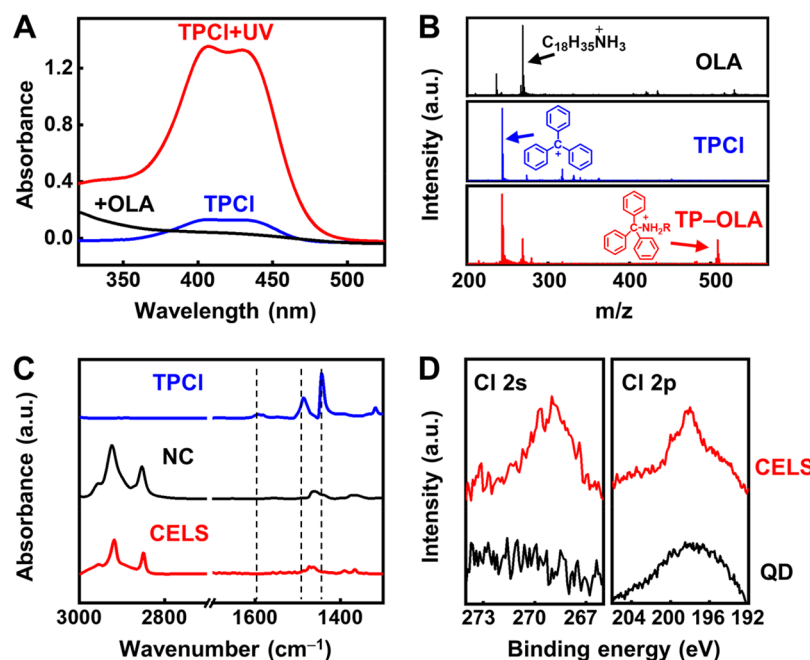


Figure 2. Underlying photochemistry of CELS. (A) UV–visible absorption spectra of TPCl before (blue) and after (red) UV irradiation at 254 nm. TP⁺ peaks occur after irradiation and disappear after the addition of OLA (black) as a result of their reaction. (B) MALDI–TOF MS of OLA, TPCl, and their Lewis adducts (TP–OLA) collected in the positive mode. The corresponding molecular ion peaks ($m/z = 268.24$, 243.04 , and 510.77 , from top to bottom) are indicated by arrows. (C) FTIR spectra of TPCl (blue), pristine OLA-capped nanocrystals (black), and CELS-treated nanocrystals (red). The dashed lines indicate the TP⁺ vibration in the benzyl region. CELS-treated nanocrystals show reduced C–H resonant peaks due to partial ligand stripping. (D) XPS Cl 2s and Cl 2p spectra of pristine and CELS-treated QDs showing efficient surface chlorination after CELS.

($C_{18}H_{35}NH_2$)⁺. During CELS, this reaction can effectively remove the native ligands from QDs. Fourier-transformed infrared (FTIR) analysis of CELS-treated Au nanocrystals (red curve in Figure 2C) shows remarkably lower C–H resonance at 2800 – 3000 cm^{-1} than pristine samples, thereby indicating the partial removal of native OLA ligands. We used OLA-capped Au nanocrystals instead of QDs in FTIR analysis because the OA ligands of QDs show overlapping resonance ($=C=O$) with TP⁺ in the benzyl region. CELS-treated QDs also show notably reduced C–H resonance. This ligand stripping process drastically reduces the solubility of QDs in nonpolar developer solvents and affords QD patterns after selective removal of QDs in unexposed regions. The degree of ligand removal will be discussed later. In an extreme case, a large excess of TPCl (over 10 times more than the ligands in molar ratio) completely removes the ligands (Figure S5). Additionally, TP–OLA adducts formed during CELS and excess TPCl are completely removed by developer solvent, as confirmed by the absence of a TP⁺ vibration in the benzyl region (Figure 2C). This excludes potential carrier or exciton traps³⁰ arising from TP⁺-containing residues.

QD surface chlorination with photogenerated Cl[−] occurs concurrently with the TP⁺–ligand reaction. CELS-treated QD films show clear Cl 2s and Cl 2p (imposed atop the broad Auger peak of Se) peaks in the X-ray photoelectron spectroscopy (XPS) spectra (Figure 2D and Figure S6). Because unreacted TPCl is thoroughly removed by developers (Figure 2C), we assigned these peaks to surface bound Cl[−] because of their strong affinity to metal sites.^{38,39}

High-Fidelity and Nondestructive QD Patterning via CELS. The chemistry of CELS enables multicolored patterning of QDs, both Cd-based and heavy-metal-free, with high

resolution, fidelity, and throughput. Typical UV doses for CELS are among 50 – 500 mJ cm^{-2} , which is comparable with those for traditional photoresists.¹³ Figure 3A–D shows fluorescent images of patterned microarrays of red, green, and blue QD layers. Additional images of QD patterns made via CELS are shown in Figure S7. The finest features are $\sim 4\text{ }\mu\text{m}$, as shown in the line patterns, which replicates those of the photomasks (Figure 3E and Figure S8). These line patterns retain uniform thickness, sharp edges (Figure 3F), and low surface roughness comparable with that of pristine, non-patterned samples (Figure 3G and Figure S9). Line edge roughness (LER) analysis (Figure S9) suggests a LER of 100 nm , which corresponds to the size of about seven QDs and is comparable with those observed for other direct photopatterning methods ($\sim 150\text{ nm}$).²⁶ In addition, the ligand stripping process does not alter the sizes of the QDs or introduce additional pinholes or cracks (Figure 3H and Figure S9) because the QD surface still contains OA ligands, although at lower coverage. Figure 3I provides an example of multicolored patterns made by consecutive QD patterning via CELS. The sizes of the RGB subpixels are $5 \times 25\text{ }\mu\text{m}$, which is relevant to a resolution >1500 pixels per inch. The patterning of the subsequent layer does not affect the morphological or optical properties of the underlying layers. CELS also works well for patterning heavy-metal-free QDs (Figure 3J–L and Figure S3G–L) and other nanocrystals (e.g., Au or CsPbBr₃) with various ligands and can be extended to other TP⁺-containing additives following similar chemistry (Figure S10).

CELS represents a nondestructive patterning method for nearly quantitative retention of the PL properties of QDs. For instance, red QD (with CdZnSe/CdZnS/ZnS core/shell/shell

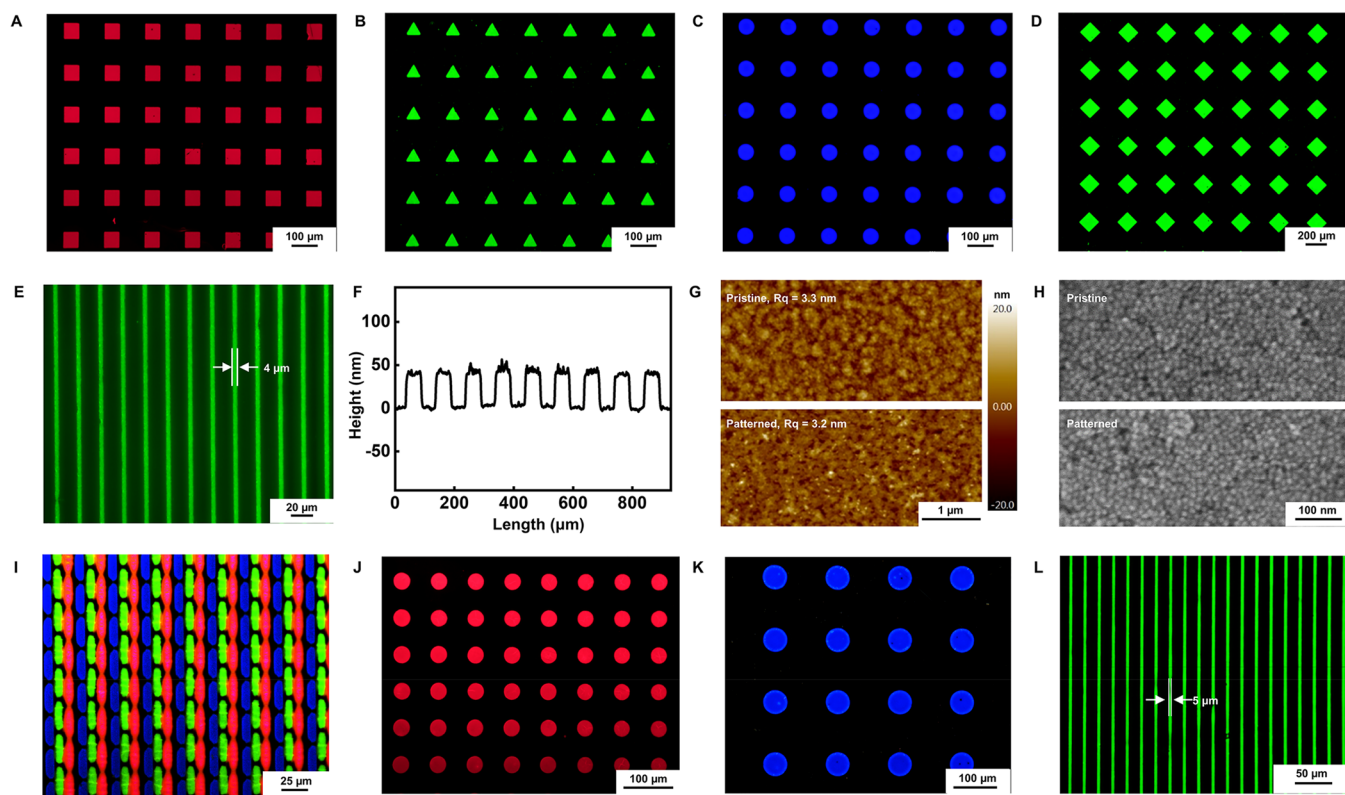


Figure 3. QD patterning via CELS. Fluorescence microscopic images of (A–D) patterned microarrays of red, green, and blue Cd-based core/shell QDs and (E) patterned lines of green QDs. (F) The height profiles of line patterns with a width/interval distance of 50 μm . (G,H) Atomic force microscopy (AFM) and scanning electron microscopy (SEM) images of pristine and CELS-patterned QD films. (I) Fluorescence microscopic images of multilayered RGB patterns made via consecutive steps. The sizes of red, green, and blue subpixels are 5 \times 25 μm . (J–L) Fluorescence images of patterns of heavy-metal-free core/shell QDs (red and green, InP/ZnS; blue, ZnSe/ZnS). Typical patterning processes use 2–10 wt % of TPCL and an exposure of 50–500 mJ cm^{-2} , depending on the QDs.

structures) films fully preserve their PLQYs at various stages of patterning (Figure 4A), including pristine, after the addition of TPCL (+TPCL), after UV exposure (in the presence of TPCL), and developed (with toluene). Figure 4B and Table S2 compare the PL decay of corresponding samples, which shows nearly identical dynamics and averaged PL lifetimes. Note, in our previous report on QD patterning via nitrene-/carbene-based photo-cross-linking chemistry,³⁰ we used the same type of red QDs, and the PLQY retention was up to 90%. This comparison highlights the nondestructive nature of CELS. Similarly, the remnant relative PLQYs of patterned green (CdZnSe/ZnSe/ZnS) and blue QD (CdZnSe/ZnS) films are ~85% and 62%, respectively (Figure S11 and Table S2). The relatively low PLQYs of patterned blue QDs may be attributed to their modest intrinsic photostability, as revealed by the shortened PL lifetime after UV exposure. We also monitored the relative PLQY changes of heavy-metal-free InP/ZnS and ZnSe/ZnS QDs with OA, OLA, and 1-dodecanethiol ligands. Although conventionally considered more vulnerable than II–VI QDs, heavy-metal-free QDs still maintain ~90% (for red and green) and 70% (for blue) of the original PLQYs after CELS (Figure 4E).

CELS further improves the photostability of QD films (Figure 4C). At the UV dose of 500 mJ cm^{-2} , CELS-treated QD films show notably higher remnant PLQYs over pristine samples (pristine and CELS: red, 82% and 97%; green, 47% and 80%; blue, 41% and 71%). Patterned green QDs maintain 44% of the original PLQYs after 1 h of continuous irradiation (6000 mJ cm^{-2} , Figure S12). To our knowledge, no previous

patterning methods were reported to improve the photostability of QDs.

The quantitative retention of PLQYs and enhanced photostability are somewhat counterintuitive because CELS relies on a ligand stripping process. Extensive studies have shown that low ligand density is related to deficient surface passivation of QDs (e.g., undercoordinated metal or chalcogenide sites) and reduced PLQYs.^{11,40,41} Proper cations and anions,^{11,40–42} introduced by ligand exchange and other processes, can passivate these surface defects via Lewis acid/base interactions, thereby leading to intense photo- or electroluminescence. To understand the microscopic origins of the unprecedented PL properties, we quantified the degree of ligand removal of red QDs (CdZnSe/CdZnS/ZnS) during CELS by using procedures described in the Supporting Information (Part 6 in Experimental Methods) and Table S3. Pristine QDs have OA as the sole surface ligand. The ligand coverage was about 3.4 nm^{-2} (or ~2000 ligands per QD) according to thermogravimetric analysis (Figure S13), which is typical for QDs with high PLQYs. During CELS, TP⁺ removed about 40% of the OA ligands (or ~800 ligands per QD) on the basis of data from gas chromatography–mass spectrometry (GC–MS) (Figure S13). The resultant ligand coverage (~2.0 nm^{-2}) was substantially lower than the density of crystalline alkane chains (4.9 nm^{-2}) on any given CdSe or ZnS facets.⁴⁰ The removal of about half the OA ligands in CELS potentially produces a considerable amount of under-coordinated Zn atoms on the QD surfaces that are unfavorable for PLQYs.

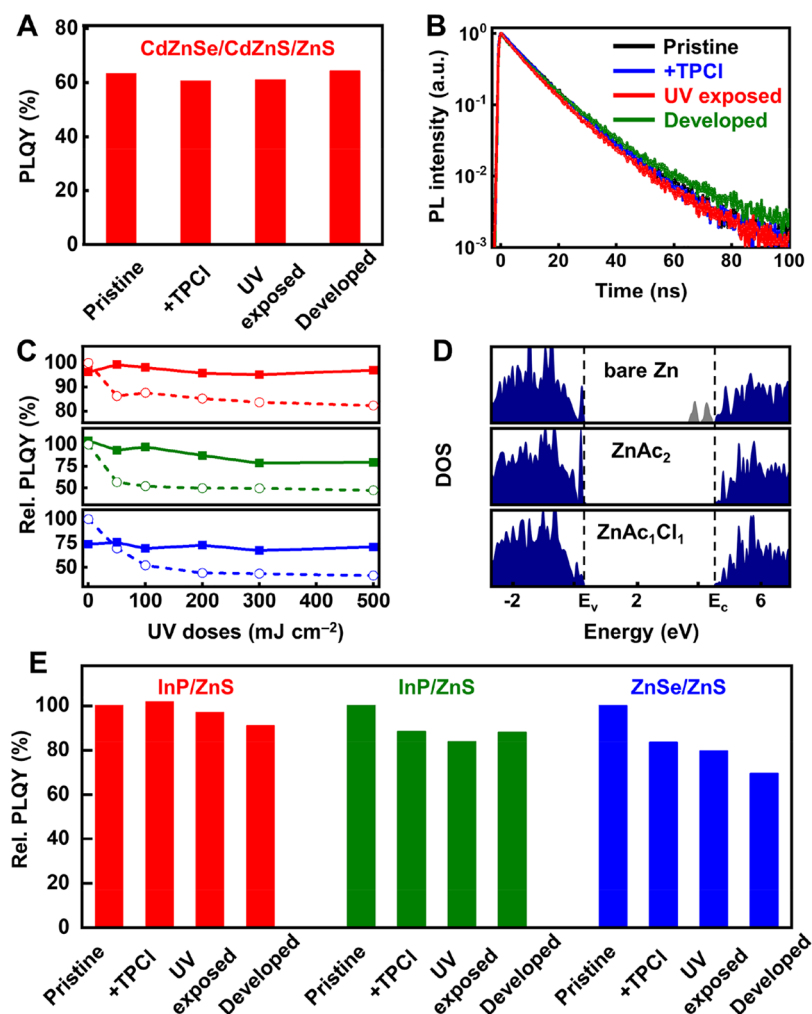


Figure 4. PL properties of CELS-patterned QDs. (A) Absolute PLQYs of red QD films remain largely unchanged at various stages of CELS, including pristine, after the addition of TPCI (+TPCI), after UV exposure in the presence of TPCI (UV exposed), and after the entire CELS procedure (developed). (B) Corresponding PL decay curves for samples shown in (A). (C) Changes in the relative PLQYs (relative to the initial PLQYs of pristine samples) of pristine (dashed lines) and CELS-patterned (solid lines) red, green, and blue QDs (from top to bottom) during UV irradiation. (D) Calculated density of states (DOS) of bare Zn, ZnAc₂, and ZnAc₁Cl₁ surfaces. Undercoordinated, bare Zn on a QD surface generates trap states (gray) near the conduction band minimum (E_c). The ZnAc₂ and ZnAc₁Cl₁ models represent the cases of pristine and CELS-treated QDs, respectively. Both show trap-state-free band gaps. E_v is the valence band maximum. (E) Changes in relative PLQYs of heavy-metal-free InP/ZnS (capped with OA and OLA ligands) and ZnSe/ZnS QD (capped with 1-dodecanethiol ligands) films at various stages for CELS. The colors of bars and curves in (A,C,E) indicate the emitting colors of corresponding QDs.

Surface chlorination may compensate this effect and provide better passivation for surface Zn atoms. Numerous reports have suggested that Cl⁻ and other halides can strongly bind to QD surfaces, eliminate midgap states, and improve the optical and electronic properties of QDs and operation stabilities of associated devices.^{11,38,39,43,44} In our case, CELS-treated QDs contain a large amount of Cl (~1100 per QD), as revealed by energy-dispersive X-ray spectroscopy (Table S3 and Figure S13) analysis. This number is comparable with that of the removed OA ligands (~800). XPS analysis shows that the molar ratio of Cl and Zn atoms (Cl/Zn) on the QD surfaces is 0.19. For reference, surface Cl/Zn is 0.18 for ZnCl₂-treated blue QDs with effective passivation and record-high EL performance.¹¹ We, thus, attributed the remarkable PL properties of CELS-treated QDs to surface chlorination.

Density functional theory (DFT) calculation corroborates the effect of surface chlorination. For simplicity, the modeled slab adopts a wurtzite ZnS (100) facet, where the Zn atoms have different surface states (Figure S14). The density of states

(DOS) of these models are shown in Figure 4D. In the absence of surface ligands (or “bare Zn”), dangling bonds introduce notable trap states (associated with nonradiative recombination pathways) near the conduction band minimum (E_c). The addition of two coordinating ligands (acetates, or Ac, which represent OA for calculation simplicity) to this slab yields fully passivated ZnAc₂ with no trap states, which is relevant to the pristine QDs with their native ligands. The replacement of half of the carboxylate ligands for Cl⁻ (ZnAc₁Cl₁) resembles the surface chemistry of CELS-treated QDs (that is, ~40% removal of OA and then passivation with an almost equal amount of Cl⁻) and does not produce trap states. Even the complete ligand exchange of Ac for Cl⁻ can maintain a trap-free band gap (Figure S14).

EL Characteristics of CELS-Patterned QLEDs. We prepared QLEDs with red, green, or blue QDs as active layers and compared their EL characteristics before and after CELS patterning. Figure 5A,B shows the device structure and energy level diagram. The active layers were made either by spin-

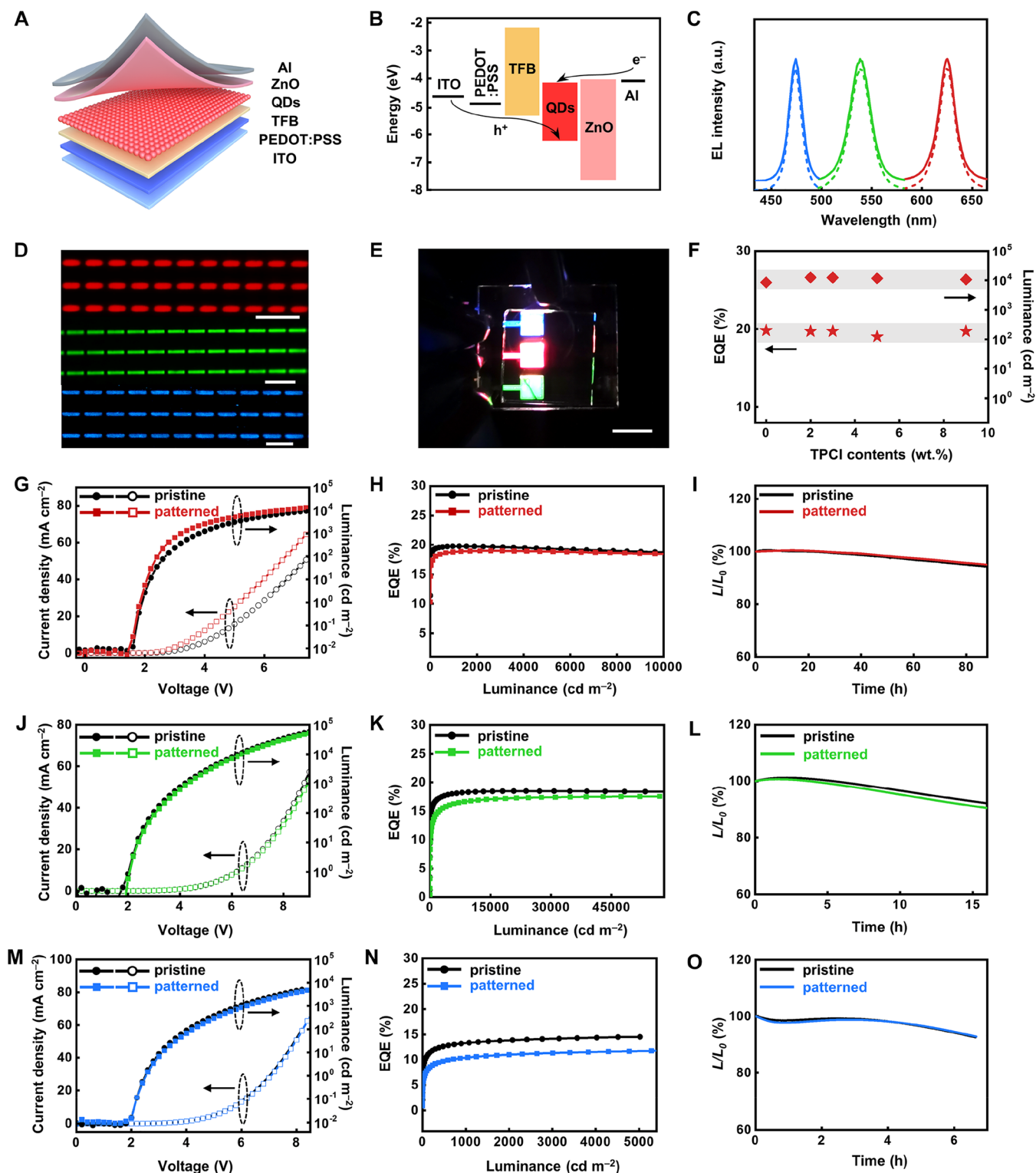


Figure 5. EL characteristics of CELS-patterned QLEDs. (A,B) Schematic device structure and energy band diagram of QLEDs. (C) Comparison of the EL spectra of pristine and patterned QLEDs. (D) EL images of pixelated red, green, and blue QD patterns. (E) EL image of consecutively patterned QLED pixels in RGB colors (scale bar, 5 mm). (F) Maximum EQEs (stars) and luminances (diamonds) of pristine and patterned red QLEDs with different TPCI contents. (G–O) J – V – L , EQEs, and temporal changes in luminance of pristine and patterned (G–I) red, (J–L) green, and (M–O) blue QLEDs.

coating the pristine QDs (pristine devices) or via CELS procedures (patterned devices). For patterned devices, unless specified, the entire QD layer was exposed for the simplicity in comparing device performance. This prevents the confounding effects, such as leakage currents because of the absence of

charge barrier materials. All device preparation procedures were performed under inert atmosphere in a nitrogen-filled glovebox.

CELS-patterned QLEDs show remarkable EQEs and operation lifetime. Pristine and patterned devices have the

same EL emission peaks (Figure 5C). Patterned red QLEDs composed of an array of $4 \times 16 \mu\text{m}$ pixels (Figure 5D and Figure S15) and consecutively patterned QLED pixels in RGB (Figure 5E) highlight the adaptability of CELS in fabricating high-definition displays. Pristine and patterned red QLEDs show almost identical EL characteristics, which are highly reproducible and insensitive to TPCL contents (within the range of 0–10 wt %) (Figure 5F and Figures S16 and S17). It supports the optimization of QD patterning capabilities by varying TPCL contents without degrading the luminescent properties. Figure 5G,H compares the current density–voltage–luminance (J – V – L) curves of pristine and patterned red QLEDs to show similar EQEs (patterned versus pristine, 19.1% versus 19.8%), current efficiency (21.0 versus 20.0 cd A $^{-1}$), and maximum luminance (13 649 versus 10 239 cd m $^{-2}$). The operation lifetime of patterned QLEDs (extrapolated T_{95} at 1000 nits, 7600 h) is almost the same as that of pristine devices (7924 h, Figure 5I). Similar comparisons apply to pristine and patterned green (Figure 5J–L) and blue (Figure 5M–O) QLEDs. Patterned devices show peak EQEs of 17.5% (green) and 12.0% (blue), and the lifetime (T_{95} at 1000 nits) for patterned green QLEDs is ~8700 h. A detailed comparison is listed in Table S4.

The EQEs and operation lifetime of CELS-patterned QLEDs exceed those reported in other patterning methods, as summarized in Table S1. Encouragingly, EL characteristics of our patterned red and green QLEDs (EQE up to ~19% and T_{95} at 1000 nits over 8000 h or T_{95} at 100 nits over 436 000 h) are also on par with the records for the state-of-the-art, nonpatterned devices. Statistics of over 20 patterned QLED devices (Figure 5F) show minimal variation in EQEs and luminance. The combined capabilities of CELS in obtaining high EL performance and high spatial resolution patterns promise its integration with optimized materials and device structures of QLEDs toward high-definition displays.

The CELS method reported here allows for building patterned QLEDs with performances contending with those of the state-of-the-art, nonpatterned devices. The dual roles of light-sensitive TPCL used in CELS chemistry facilitate the partial stripping of native ligands by TP $^{+}$ and surface chlorination by Cl $^{-}$, which produces high-resolution QD patterns with fully preserved PLQYs and improved photostability. The preserved photophysical properties of patterned QD layers translate to high efficiency and a long operation lifetime in patterned QLEDs. Further developments on CELS include the design of photosensitive chemicals with a similar reaction mechanism but improved patterning capabilities. We expect CELS to bridge the performance gap between individual devices and patterned QLEDs for realizing high-performance QLED displays and other integrated device platforms.

■ ASSOCIATED CONTENT

SI Supporting Information

The Supporting Information is available free of charge at <https://pubs.acs.org/doi/10.1021/acs.nanolett.3c00146>.

Experimental methods; absorption spectrum of TPCL; optical spectra and TEM images of QDs; additional mass spectra of TPCL, OLA and their adducts; characterizations of ligand-stripped QDs; additional XPS data; optical, SEM, and AFM images of QD patterns; PL properties of patterned QDs; character-

izations on the ratio of stripped ligands and surface chlorination; configurations and DOS of ZnS surface used in DFT; additional EL characteristics and images of patterned QLEDs; tables on the quantitative analysis of surface chemistry during CELS; and comparison of EL characteristics of CELS-patterned QLEDs with those by other patterning methods (PDF)

■ AUTHOR INFORMATION

Corresponding Authors

Hao Zhang – Department of Chemistry, Center for BioAnalytical Chemistry, Key Laboratory of Bioorganic Phosphorus Chemistry & Chemical Biology of Ministry of Education, Tsinghua University, Beijing 100084, China; Laboratory of Flexible Electronic Technology, Tsinghua University, Beijing 100084, China;  orcid.org/0000-0003-4513-0813; Email: hzhangchem@mail.tsinghua.edu.cn

Jinghong Li – Department of Chemistry, Center for BioAnalytical Chemistry, Key Laboratory of Bioorganic Phosphorus Chemistry & Chemical Biology of Ministry of Education, Tsinghua University, Beijing 100084, China;  orcid.org/0000-0002-0750-7352; Email: jqli@mail.tsinghua.edu.cn

Authors

Zhong Fu – Department of Chemistry, Center for BioAnalytical Chemistry, Key Laboratory of Bioorganic Phosphorus Chemistry & Chemical Biology of Ministry of Education, Tsinghua University, Beijing 100084, China

Likuan Zhou – TCL Research, Shenzhen, Guangdong 518067, China

Yue Yin – Department of Chemistry, Center for BioAnalytical Chemistry, Key Laboratory of Bioorganic Phosphorus Chemistry & Chemical Biology of Ministry of Education, Tsinghua University, Beijing 100084, China;  orcid.org/0000-0002-9390-3983

Kangkang Weng – Department of Chemistry, Center for BioAnalytical Chemistry, Key Laboratory of Bioorganic Phosphorus Chemistry & Chemical Biology of Ministry of Education, Tsinghua University, Beijing 100084, China

Fu Li – Department of Chemistry, Center for BioAnalytical Chemistry, Key Laboratory of Bioorganic Phosphorus Chemistry & Chemical Biology of Ministry of Education, Tsinghua University, Beijing 100084, China

Shaoyong Lu – Department of Chemistry, Center for BioAnalytical Chemistry, Key Laboratory of Bioorganic Phosphorus Chemistry & Chemical Biology of Ministry of Education, Tsinghua University, Beijing 100084, China

Dan Liu – Department of Chemistry, Center for BioAnalytical Chemistry, Key Laboratory of Bioorganic Phosphorus Chemistry & Chemical Biology of Ministry of Education, Tsinghua University, Beijing 100084, China

Wenyoung Liu – TCL Research, Shenzhen, Guangdong 518067, China

Longjia Wu – TCL Research, Shenzhen, Guangdong 518067, China

Yixing Yang – TCL Research, Shenzhen, Guangdong 518067, China

Haifang Li – Department of Chemistry, Center for BioAnalytical Chemistry, Key Laboratory of Bioorganic Phosphorus Chemistry & Chemical Biology of Ministry of Education, Tsinghua University, Beijing 100084, China;  orcid.org/0000-0002-0447-4655

Lian Duan — Department of Chemistry, Center for BioAnalytical Chemistry, Key Laboratory of Bioorganic Phosphorus Chemistry & Chemical Biology of Ministry of Education, Tsinghua University, Beijing 100084, China; Laboratory of Flexible Electronic Technology, Tsinghua University, Beijing 100084, China

Hai Xiao — Department of Chemistry, Center for BioAnalytical Chemistry, Key Laboratory of Bioorganic Phosphorus Chemistry & Chemical Biology of Ministry of Education, Tsinghua University, Beijing 100084, China;  orcid.org/0000-0001-9399-1584

Complete contact information is available at:
<https://pubs.acs.org/10.1021/acs.nanolett.3c00146>

Author Contributions

The manuscript was written through the contributions of all authors. H.Z. conceived the concept of this work. H.Z. and Z.F. designed the experimental work, analyzed the data, and cowrote the paper. Z.F. led the experimental work with support from K.W., F.L., S.L., D.L., and H.L. Y.Yin performed simulations under the supervision of H.X. and with assistance from Z.F. K.W. performed preliminary QLED tests under the supervision of L.D. L.Z. prepared and characterized the QLED devices under the supervision of W.L., L.W., and Y.Yang. H.Z. and J.L. supervised the project.

Notes

The authors declare no competing financial interest.

ACKNOWLEDGMENTS

This work was financially supported by the National Natural Science Foundation of China (No. 21974079 and No. 22274087) (H.Z.), Tsinghua University Dushi Program (H.Z.), the Strategic Priority Research Program of Chinese Academy of Sciences (No. XDB36000000) (J.L.), the International Scientific Partnership Program [No. ISPP-20-155(1)] (J.L.), and the Pearl River Talent Recruitment Program for Guangdong Introducing Innovative and Entrepreneurial Teams (No. 2016ZT06C650) (L.Z., W.L., L.W., Y.Yang).

REFERENCES

- (1) García de Arquer, F. P.; Talapin, D. V.; Klimov, V. I.; Arakawa, Y.; Bayer, M.; Sargent, E. H. Semiconductor quantum dots: Technological progress and future challenges. *Science* **2021**, *373* (6555), No. eaaz8541.
- (2) Liu, M.; Yazdani, N.; Yarema, M.; Jansen, M.; Wood, V.; Sargent, E. H. Colloidal quantum dot electronics. *Nat. Electron.* **2021**, *4* (8), 548–558.
- (3) Kagan, C. R.; Lifshitz, E.; Sargent, E. H.; Talapin, D. V. Building devices from colloidal quantum dots. *Science* **2016**, *353* (6302), aac5523.
- (4) Efros, A. L.; Brus, L. E. Nanocrystal quantum dots: From discovery to modern development. *ACS Nano* **2021**, *15* (4), 6192–6210.
- (5) Yang, J.; Choi, M. K.; Yang, U. J.; Kim, S. Y.; Kim, Y. S.; Kim, J. H.; Kim, D.-H.; Hyeon, T. Toward full-color electroluminescent quantum dot displays. *Nano Lett.* **2021**, *21* (1), 26–33.
- (6) Shirasaki, Y.; Supran, G. J.; Bawendi, M. G.; Bulovic, V. Emergence of colloidal quantum-dot light-emitting technologies. *Nat. Photonics* **2013**, *7* (1), 13–23.
- (7) Cho, K.-S.; Lee, E. K.; Joo, W.-J.; Jang, E.; Kim, T.-H.; Lee, S. J.; Kwon, S.-J.; Han, J. Y.; Kim, B.-K.; Choi, B. L.; Kim, J. M. High-performance crosslinked colloidal quantum-dot light-emitting diodes. *Nat. Photonics* **2009**, *3* (6), 341–345.
- (8) Yang, Y.; Zheng, Y.; Cao, W.; Titov, A.; Hyvonen, J.; Manders, J. R.; Xue, J.; Holloway, P. H.; Qian, L. High-efficiency light-emitting devices based on quantum dots with tailored nanostructures. *Nat. Photonics* **2015**, *9* (4), 259–266.
- (9) Dai, X.; Zhang, Z.; Jin, Y.; Niu, Y.; Cao, H.; Liang, X.; Chen, L.; Wang, J.; Peng, X. Solution-processed, high-performance light-emitting diodes based on quantum dots. *Nature* **2014**, *515* (7525), 96–99.
- (10) Li, X.; Lin, Q.; Song, J.; Shen, H.; Zhang, H.; Li, L. S.; Li, X.; Du, Z. Quantum-dot light-emitting diodes for outdoor displays with high stability at high brightness. *Adv. Optical Mater.* **2020**, *8* (2), 1901145.
- (11) Kim, T.; Kim, K.-H.; Kim, S.; Choi, S.-M.; Jang, H.; Seo, H.-K.; Lee, H.; Chung, D.-Y.; Jang, E. Efficient and stable blue quantum dot light-emitting diode. *Nature* **2020**, *586* (7829), 385–389.
- (12) Pu, C.; Dai, X.; Shu, Y.; Zhu, M.; Deng, Y.; Jin, Y.; Peng, X. Electrochemically-stable ligands bridge the photoluminescence-electroluminescence gap of quantum dots. *Nat. Commun.* **2020**, *11* (1), 937.
- (13) Wang, Y.; Fedin, I.; Zhang, H.; Talapin, D. V. Direct optical lithography of functional inorganic nanomaterials. *Science* **2017**, *357* (6349), 385–388.
- (14) Palazon, F.; Prato, M.; Manna, L. Writing on nanocrystals: Patterning colloidal inorganic nanocrystal films through irradiation-induced chemical transformations of surface ligands. *J. Am. Chem. Soc.* **2017**, *139* (38), 13250–13259.
- (15) Hu, C.; Aubert, T.; Justo, Y.; Flamee, S.; Cirillo, M.; Gassenq, A.; Drobchak, O.; Beunis, F.; Roelkens, G.; Hens, Z. The micropatterning of layers of colloidal quantum dots with inorganic ligands using selective wet etching. *Nanotechnology* **2014**, *25* (17), 175302.
- (16) Park, J.-S.; Kyhm, J.; Kim, H. H.; Jeong, S.; Kang, J.; Lee, S.-E.; Lee, K.-T.; Park, K.; Barange, N.; Han, J.; Song, J. D.; Choi, W. K.; Han, I. K. Alternative patterning process for realization of large-area, full color, active quantum dot display. *Nano Lett.* **2016**, *16* (11), 6946–6953.
- (17) Kim, T.-H.; Cho, K.-S.; Lee, E. K.; Lee, S. J.; Chae, J.; Kim, J. W.; Kim, D. H.; Kwon, J.-Y.; Amaralunga, G.; Lee, S. Y.; Choi, B. L.; Kuk, Y.; Kim, J. M.; Kim, K. Full-Color Quantum Dot Displays Fabricated by Transfer Printing. *Nat. Photonics* **2011**, *5* (3), 176–182.
- (18) Choi, M. K.; Yang, J.; Kang, K.; Kim, D. C.; Choi, C.; Park, C.; Kim, S. J.; Chae, S. I.; Kim, T. H.; Kim, J. H.; Hyeon, T.; Kim, D. H. Wearable red-green-blue quantum dot light-emitting diode array using high-resolution intaglio transfer printing. *Nat. Commun.* **2015**, *6* (1), 7149.
- (19) Xiang, C.; Wu, L.; Lu, Z.; Li, M.; Wen, Y.; Yang, Y.; Liu, W.; Zhang, T.; Cao, W.; Tsang, S. W.; Shan, B.; Yan, X.; Qian, L. High efficiency and stability of ink-jet printed quantum dot light emitting diodes. *Nat. Commun.* **2020**, *11* (1), 1646.
- (20) Zhao, J.; Chen, L.; Li, D.; Shi, Z.; Liu, P.; Yao, Z.; Yang, H.; Zou, T.; Zhao, B.; Zhang, X.; Zhou, H.; Yang, Y.; Cao, W.; Yan, X.; Zhang, S.; Sun, X. W. Large-area patterning of full-color quantum dot arrays beyond 1000 pixels per inch by selective electrophoretic deposition. *Nat. Commun.* **2021**, *12* (1), 4603.
- (21) Xing, X.; Man, Z.; Bian, J.; Yin, Y.; Zhang, W.; Lu, Z. High-resolution combinatorial patterning of functional nanoparticles. *Nat. Commun.* **2020**, *11* (1), 6002.
- (22) Nam, T. W.; Kim, M.; Wang, Y.; Kim, G. Y.; Choi, W.; Lim, H.; Song, K. M.; Choi, M.-J.; Jeon, D. Y.; Grossman, J. C.; Jung, Y. S. Thermodynamic-driven polychromatic quantum dot patterning for light-emitting diodes beyond eye-limiting resolution. *Nat. Commun.* **2020**, *11* (1), 3040.
- (23) Meng, T.; Zheng, Y.; Zhao, D.; Hu, H.; Zhu, Y.; Xu, Z.; Ju, S.; Jing, J.; Chen, X.; Gao, H.; Yang, K.; Guo, T.; Li, F.; Fan, J.; Qian, L. Ultrahigh-resolution quantum-dot light-emitting diodes. *Nat. Photonics* **2022**, *16* (4), 297–303.
- (24) Wang, Y.; Pan, J.-A.; Wu, H.; Talapin, D. V. Direct wavelength-selective optical and electron-beam lithography of functional inorganic nanomaterials. *ACS Nano* **2019**, *13* (12), 13917–13931.

- (25) Cho, H.; Pan, J. A.; Wu, H.; Lan, X.; Coropceanu, I.; Wang, Y.; Cho, W.; Hill, E. A.; Anderson, J. S.; Talapin, D. V. Direct optical patterning of quantum dot light-emitting diodes via *in situ* ligand exchange. *Adv. Mater.* **2020**, *32* (46), 2003805.
- (26) Yang, J.; Hahm, D.; Kim, K.; Rhee, S.; Lee, M.; Kim, S.; Chang, J. H.; Park, H. W.; Lim, J.; Lee, M.; Kim, H.; Bang, J.; Ahn, H.; Cho, J. H.; Kwak, J.; Kim, B.; Lee, C.; Bae, W. K.; Kang, M. S. High-resolution patterning of colloidal quantum dots via non-destructive, light-driven ligand crosslinking. *Nat. Commun.* **2020**, *11* (1), 2874.
- (27) Hahm, D.; Lim, J.; Kim, H.; Shin, J.-W.; Hwang, S.; Rhee, S.; Chang, J. H.; Yang, J.; Lim, C. H.; Jo, H.; Choi, B.; Cho, N. S.; Park, Y.-S.; Lee, D. C.; Hwang, E.; Chung, S.; Kang, C.-m.; Kang, M. S.; Bae, W. K. Direct patterning of colloidal quantum dots with adaptable dual-ligand surface. *Nat. Nanotechnol.* **2022**, *17* (9), 952–958.
- (28) Yang, J.; Lee, M.; Park, S. Y.; Park, M.; Kim, J.; Sitapure, N.; Hahm, D.; Rhee, S.; Lee, D.; Jo, H.; Jo, Y. H.; Lim, J.; Kim, J.; Shin, T. J.; Lee, D. C.; Kwak, K.; Kwon, J. S.; Kim, B.; Bae, W. K.; Kang, M. S. Nondestructive Photopatterning of Heavy-Metal-Free Quantum Dots. *Adv. Mater.* **2022**, *34* (43), 2205504.
- (29) Liu, D.; Weng, K.; Lu, S.; Li, F.; Abudukeremu, H.; Zhang, L.; Yang, Y.; Hou, J.; Qiu, H.; Fu, Z.; Luo, X.; Duan, L.; Zhang, Y.; Zhang, H.; Li, J. Direct optical patterning of perovskite nanocrystals with ligand crosslinkers. *Sci. Adv.* **2022**, *8* (11), No. eabm8433.
- (30) Lu, S.; Fu, Z.; Li, F.; Weng, K.; Zhou, L.; Zhang, L.; Yang, Y.; Qiu, H.; Liu, D.; Qing, W.; Ding, H.; Sheng, X.; Chen, M.; Tang, X.; Duan, L.; Liu, W.; Wu, L.; Yang, Y.; Zhang, H.; Li, J. Beyond a linker: The role of photochemistry of crosslinkers in the direct optical patterning of colloidal nanocrystals. *Angew. Chem., Int. Ed.* **2022**, *61* (23), No. e202202633.
- (31) Huang, J.; Liu, W.; Dolzhnikov, D. S.; Protesescu, L.; Kovalenko, M. V.; Koo, B.; Chattopadhyay, S.; Shchenko, E. V.; Talapin, D. V. Surface functionalization of semiconductor and oxide nanocrystals with small inorganic oxoanions (PO_4^{3-} , MoO_4^{2-}) and polyoxometalate ligands. *ACS Nano* **2014**, *8* (9), 9388–9402.
- (32) McClelland, R. A.; Banait, N.; Steenken, S. Electrophilic Reactivity of the Triphenylmethyl Carbocation in Aqueous Solutions. *J. Am. Chem. Soc.* **1986**, *108* (22), 7023–7027.
- (33) Shah, P. S.; Holmes, J. D.; Johnston, K. P.; Korgel, B. A. Size-selective dispersion of dodecanethiol-coated nanocrystals in liquid and supercritical ethane by density tuning. *J. Phys. Chem. B* **2002**, *106* (10), 2545–2551.
- (34) Yang, Y.; Qin, H.; Peng, X. Intramolecular entropy and size-dependent solution properties of nanocrystal–ligands complexes. *Nano Lett.* **2016**, *16* (4), 2127–2132.
- (35) Jones, R. L.; Dorfman, L. M. Submicrosecond formation and observation of reactive carbonium ions. *J. Am. Chem. Soc.* **1974**, *96* (18), 5715–5722.
- (36) Yoshida, S.; Shimomori, K.; Kim, Y.; Hosoya, T. Single C–F bond cleavage of trifluoromethylarenes with an ortho-silyl group. *Angew. Chem., Int. Ed.* **2016**, *55* (35), 10406–10409.
- (37) Idogawa, R.; Kim, Y.; Shimomori, K.; Hosoya, T.; Yoshida, S. Single C–F transformations of o-hydrosilyl benzotrifluorides with trityl compounds as all-in-one reagents. *Org. Lett.* **2020**, *22* (23), 9292–9297.
- (38) Zhang, H.; Dasbiswas, K.; Ludwig, N. B.; Han, G.; Lee, B.; Vaikuntanathan, S.; Talapin, D. V. Stable colloids in molten inorganic salts. *Nature* **2017**, *542* (7641), 328–331.
- (39) Zhang, H.; Jang, J.; Liu, W.; Talapin, D. V. Colloidal nanocrystals with inorganic halide, pseudohalide, and halometallate ligands. *ACS Nano* **2014**, *8* (7), 7359–7369.
- (40) Anderson, N. C.; Hendricks, M. P.; Choi, J. J.; Owen, J. S. Ligand exchange and the stoichiometry of metal chalcogenide nanocrystals: Spectroscopic observation of facile metal-carboxylate displacement and binding. *J. Am. Chem. Soc.* **2013**, *135* (49), 18536–18548.
- (41) Kirkwood, N.; Monchen, J. O. V.; Crisp, R. W.; Grimaldi, G.; Bergstein, H. A. C.; Du Fossé, I.; Van der stam, W.; Infante, I.; Houtepen, A. J. Finding and fixing traps in II–VI and III–V colloidal quantum dots: the importance of Z-type ligand passivation. *J. Am. Chem. Soc.* **2018**, *140* (46), 15712–15723.
- (42) Xiao, P.; Zhang, Z.; Ge, J.; Deng, Y.; Chen, X.; Zhang, J. R.; Deng, Z.; Kambe, Y.; Talapin, D. V.; Wang, Y. Surface passivation of intensely luminescent all-inorganic nanocrystals and their direct optical patterning. *Nat. Commun.* **2023**, *14* (1), 49.
- (43) Ip, A. H.; Thon, S. M.; Hoogland, S.; Voznyy, O.; Zhitomirsky, D.; Debnath, R.; Levina, L.; Rollny, L. R.; Carey, G. H.; Fischer, A.; Kemp, K. W.; Kramer, I. J.; Ning, Z.; Labelle, A. J.; Chou, K. W.; Amassian, A.; Sargent, E. H. Hybrid passivated colloidal quantum dot solids. *Nat. Nanotechnol.* **2012**, *7* (9), 577–582.
- (44) Li, X.; Zhao, Y.-B.; Fan, F.; Levina, L.; Liu, M.; Quintero-Bermudez, R.; Gong, X.; Quan, L. N.; Fan, J.; Yang, Z.; Hoogland, S.; Voznyy, O.; Lu, Z.-H.; Sargent, E. H. Bright collidal quantum dots light-emitting diodes enabled by efficient chlorination. *Nat. Photonics* **2018**, *12* (3), 159–164.

□ Recommended by ACS

Patterning Perovskite Quantum Dots Using Photopolymerization

Mamoru Morinaga, Hideyuki Nakanishi, et al.

FEBRUARY 22, 2023

ACS APPLIED MATERIALS & INTERFACES

READ ↗

Canny Algorithm Enabling Precise Offline Line Edge Roughness Acquisition in High-Resolution Lithography

Ziyu Hu, Xiangming He, et al.

JANUARY 18, 2023

ACS OMEGA

READ ↗

Area-Specific, Hierarchical Nanowrinkling of Two-Dimensional Materials

Dongjoon Rhee, Teri W. Odom, et al.

MARCH 29, 2023

ACS NANO

READ ↗

Subnanometer-Wide Indium Selenide Nanoribbons

William J. Cull, Andrei N. Khlobystov, et al.

MARCH 14, 2023

ACS NANO

READ ↗

Get More Suggestions >